İSTANBUL UNIVERSITY
CERRAHPAŞA

ORIGINAL ARTICLE
Electrica 2024; 24(2): 542-551

A New Modeling Method for the Electromagnetic Emission of Integrated Circuits

Muhammed Emin Başak[1], Ayten Kuntman[2]

[1]Department of Marine Engineering, Yıldız Technical University, Faculty of Naval Architecture and Maritime, İstanbul, Türkiye
[2]Department of Electrical and Electronics Engineering, İstanbul University-Cerrahpaşa, Faculty of Engineering, İstanbul, Türkiye

Cite this article as: M. Emin Başak and A. Kuntman, "A new modeling method for the electromagnetic emission of integrated circuits," *Electrica*, 24(2), 542-551, 2024.

ABSTRACT

A new method for estimating the parasitic emission of integrated circuits (ICs) is the main objective of this paper. In this study, experimental circuits were formulated, and printed circuit boards were fabricated to evaluate the input impedance at the power supply terminal of the designated microcontroller. Following the measurement of S-parameters for the experimental setup across a frequency spectrum ranging from 10 MHz to 2 GHz, Z-parameters were derived from the acquired S-parameter data. Then, all the unwanted impedance effects on the conducted line have been deleted mathematically with the de-embedding technique. The passive Resistor Inductor Capacitor (RLC) circuit was extracted using both analytic and modified genetic algorithms. Subsequently, the internal current values of the power supply pins were determined. Afterwards the passive RLC circuit and internal current values were obtained; the magnetic field in the internal structure of the IC was modeled as uniformly distributed conductive lines. The locations of the uniformly distributed conductive lines on the IC are defined as a straight route from the ends of the power supply pin to the IC core according to measurement results. A series of electromagnetic near-field measurements were conducted at varying frequencies in order to investigate the currents that traverse the power supply pins. The simulation of the magnetic field is conducted across the circuit under examination at varying frequencies and altitudes. The model results were compared to the measurement results obtained using the near-field test bench, which demonstrated a high degree of correlation.

***Index Terms*—**Conducted emissions, electromagnetic, integrated circuits

Corresponding author:
Muhammed Emin Başak

E-mail:
mebasak@yildiz.edu.tr

Received: April 26, 2024

Revision Requested: May 22, 2024

Last Revision Received: May 22, 2024

Accepted: May 22, 2024

Publication Date: May 31, 2024

DOI: 10.5152/electrica.2024.24053

I. INTRODUCTION

Different studies all around the world are being carried out in order to obtain a methodology that allows the prediction of electromagnetic emissions and interferences in order to control them. For this reason, industries are interested in the electromagnetic models and in particular the automotive and aeronautical sectors. The technological progresses enabled the miniaturization of integrated circuits (ICs), and interference problems related to emissions become more important. In order to ensure that the circuits work together without risk and correctly and to meet the electromagnetic compatibility (EMC) standards, an accurate knowledge of their electromagnetic environment is necessary. In a typical electronic system, the voltage or current caused by conditions is more susceptible to damage the ICs. Although ICs typically serve as the primary source or recipient of EMC issues, many EMC-focused researchers and problem-solvers have traditionally focused on factors external to the IC package. Various simulation tools enable the anticipation of device behavior and identification of potential operational irregularities within their proximate environment. However, relying solely on these tools may prove inadequate for analyzing active circuits or intricate systems. Consequently, numerous models have been suggested to elucidate the EMC characteristics of an IC and facilitate emissions simulation [1–4].

Electromagnetic compatibility problems at the component level are important to be analyzed early in the circuit and component design because the generated noise from the ICss will cause problems for the external world if they are ignored. With the advancement of IC performance, the proliferation of clock systems, and the acceleration of transition times, ICs are increasingly becoming the primary contributors to the electromagnetic behavior exhibited by electronic equipment and systems. Consequently, as technology scales down, the prevalence of parasitic emissions rises. To address this issue, numerous studies worldwide are underway to develop methodologies enabling the prediction and control of electromagnetic emissions and interferences. For this reason, different companies are interested in the electromagnetic models. The proposed model

makes it possible to simulate the emission of ICs even if the data from the IC manufacturer is not available. For example, Zhang and Bazzi [5] discuss the background and motivation for the design, the design methodology, and the simulation and experimental results. The proposed model is shown to be effective in reducing conducted EMI on both alternate- and direct-current power lines.

The different methods and strategies were presented for reducing the EMI emitted by the ICs. The first important contribution of the components of EMC modeling is input/output buffer information specification (IBIS) [2]. Nevertheless, the IBIS model does not consider the primary sources of IC parasitic emission currents, which are induced in the IC supply network by the switching of input/output (I/O) buffers and the internal activity (IA) of the component [5–15]. Synchronically, the I/O interface model of the IC was also developed [6]. The linear equivalent circuit and current source (LECCS) model [7] has also been proposed for the prediction of emissions and immunity tasks [8]. Integrated circuit emission model (ICEM) is the other method to predict the electromagnetic emission of IC [9–13]. The objective of the ICEM model is to propose a new approach to electrical modeling for IC internal activities. The electromagnetic behavior and performance of electronic devices have been extracted using these models. The models previously described permit producers to test their products and collect data on the electromagnetic performance of their circuits, while maintaining confidentiality regarding their products [12]. Furthermore, system suppliers can leverage this information to ensure that emissions remain within the bounds of their specifications. In the future, EMC engineers will need to address the challenge of developing, testing, and modeling methods capable of addressing the fundamental complexities of the evolving electromagnetic environment within ICs, all while minimizing cost and time delays.

Various methodologies have been documented in the literature [14] for calculating emissions from ICs. Consequently, a range of formulations for representation and diverse approaches for modeling the magnetic field have been detailed [14–16]. Kralicek and others [14] proposed a multipole expansion to demonstrate the suitability of physically based emission macro-models of IC for development and use in tools for system-level analysis. The modal expansion method, as applied to antenna studies [17, 18], involves taking the two-dimensional (2-D) Fast Fourier Transform (FFT) of the measurement data to reach the far field. This is followed by the calculation of equivalent currents on the source plane, and finally, the generation of a set of magnetic and/or electric dipoles. Genetic and metaheuristic algorithms have also been employed to calculate the parameters of the model for applications of EMC. While iterative methods are effective, they require a significant amount of time to complete, with a typical modeling process taking approximately 4 hours [19, 20]. Vives Gilabert and others [19] have proposed a methodology to characterize radiated emissions. The approach was based on a set of electric elemental dipoles, which required the measurement of two components of the magnetic field, H_x and H_y. In this case, the dipoles were also disposed in the same plane; however, in this approach, the process of modeling was able to calculate the orientation of each dipole in the plane and the value of the current. The aforementioned process is dependent on the number of points of measurement and the number of dipoles, with the time required for completion varying accordingly. However, it is notable that the process was considerably more expedient than that of an iterative model.

The aim of this paper is to present data for calculating the electromagnetic field generated by an IC. To achieve this goal, a test circuit incorporating the MC9S12X microcontroller was devised, and measurements were conducted. Due to the fact that it was difficult to obtain the correct results from the original board owing to the fact that traces and the board properties were not known exactly, the new board was designed for making the power delivery network (PDN) measurement. The network analyzer was utilized to conduct measurements on the prepared test circuit, with no voltage applied to the circuit during the testing process. Following the measurement of the S-parameters for the test circuit within the frequency range of 10 MHz to 2 GHz, the Z-parameters were derived from the S-parameters. Following the removal of impedance effects through de-embedding, the passive RLC circuit was excluded from the measurement. The detailed methodology is outlined in [4]. Second, the measurement has been performed to obtain the external current. This current and passive distribution network was used to calculate the internal activity required in the ICEM model. The values for the different frequencies have been obtained. In order to ascertain the current within the power supply, it is essential to define the impedance characteristics of the passive supply network and the profile of the instantaneous current drawn by the chip core. Subsequently, the model is constructed using lines of current defined by their magnitude and orientation within the plane. Once the sources are established, the magnetic field emitted at any distance from the device can be calculated. Both the impedance of the power supply network and the current at the power supply pin have been analyzed to ascertain the instantaneous current consumed by the chip core. After the uniformly distributed current lines to (a plane surface) by using MATLAB codes, the electromagnetic field can be simulated at the different frequencies. The model relies on a series of current lines that replace the electronic circuit. Magnetic field simulations are conducted at various frequencies (24, 32, and 64 MHz) and heights ($h = 1$ mm and $h = 4$ mm) above the circuit under examination, with subsequent comparison to the measured values.

II. MODELLING OF THE PASSIVE RLC CIRCUIT

In this research, the S12X microcontroller, a 16-bit microcontroller manufactured by Freescale Semiconductor, was employed. Widely utilized in automotive electronic systems, this IC is fabricated using 0.25 μm CMOS technology. Featuring eight pairs of power and ground pins, it supplies power to various components including the I/O ports, A/D converter, oscillator, phase-locked loop (PLL), and digital core. The microcontroller is packaged in a thin quad flat pack with 144 pins [11]. The study conducted power supply input impedance measurements utilizing the ICEM and LECCS model standards.

Measurement configuration of PDN and designed test circuit included in S12X microcontroller is shown in Fig. 1. Several tests have been done and impedances of all of the power supply are presented in Table I. In this study, the measurement specifics concerning the VddPLL and VssPLL (power and ground) pins are elaborated. It is important to note that the measurement and calculations for all other supply and ground pins were conducted using the same methodology. The measurement configuration is shown in Fig. 2.

For practical reasons, initially S parameters were measured, which were subsequently converted to Z parameters. Following the measurements, the impedance model was derived, indicating a first-order resonance and yielding the global resistance value R at the resonance frequency. However, before establishing the impedance

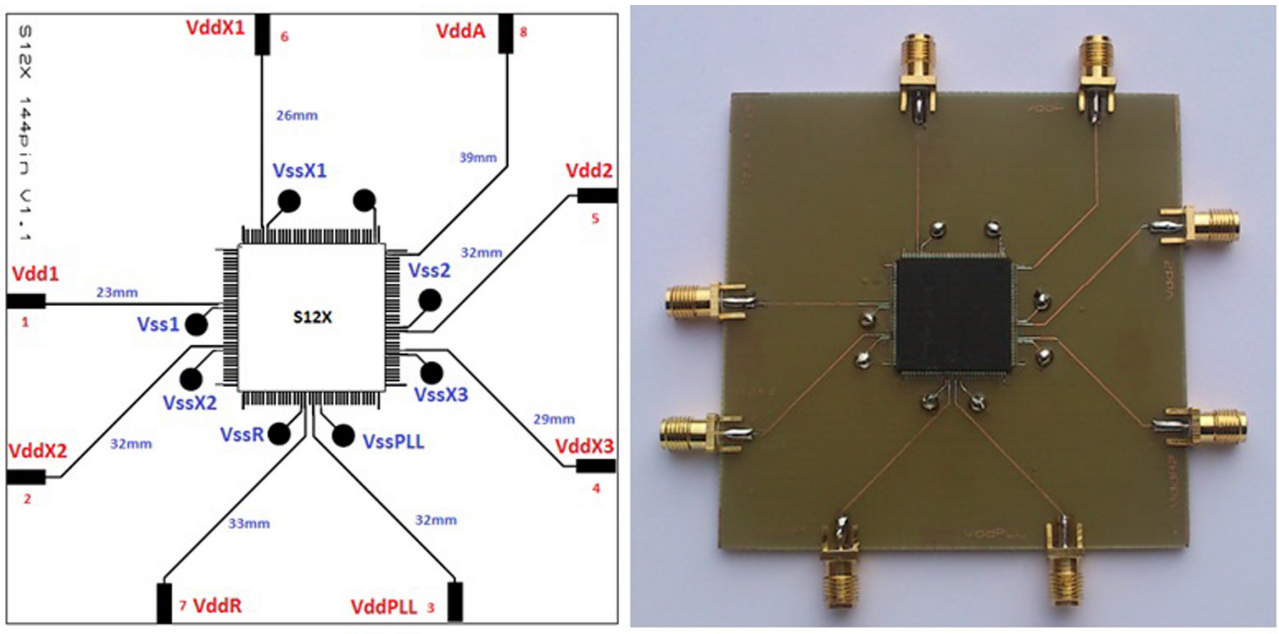

Fig. 1. Designed test circuit including S12X microcontroller.

TABLE I. INTERNAL ACTIVITY CURRENT VALUES ACCORDING TO CONSTANT EXTERNAL CURRENT VALUES

I_{int}(mA)	V_{dd1} (mA)	V_{ddX2} (mA)	V_{ddPLL} (mA)	V_{ddR2} (mA)	V_{dd2} (mA)	V_{ddX1} (mA)	V_{ddR1} (mA)	V_{ddA} (mA)
24 MHz	1.7	0.51	0.50	0.51	1.6	0.5	0.68	0.52
32 MHz	2.4	0.54	0.53	0.55	2.2	0.52	0.81	0.56
64 MHz	6.8	0.72	0.67	0.77	0.44	0.68	1.6	0.76

model, de-embedding to eliminate the effects of traces was performed. De-embedding is a mathematical process that removes the influence of unwanted structural components embedded in the measured data by subtracting their contribution. It is important to note that traces on the board can have a more significant impact on the measured data than the device under test (DUT) itself [21]. Before applying the de-embedding process, the traces which are seen between the IC core and the power supply pin were measured by the microscope. The microscopic vision of the VddPLL power supply path is shown in Fig. 3. The effects of the trace to the circuit is shown in Fig. 4.

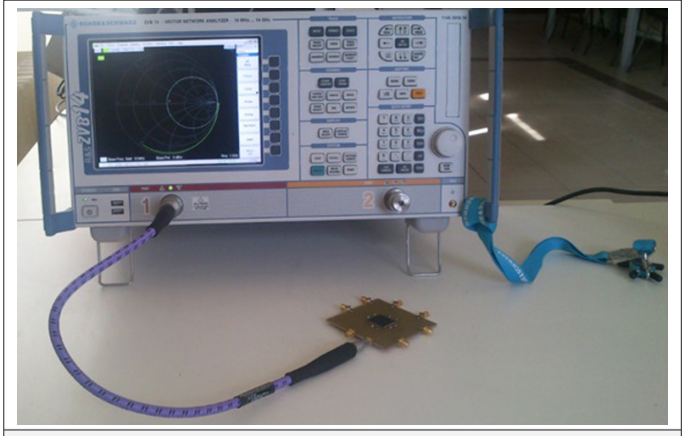

Fig. 2. Measurement configuration of passive RLC circuit.

Measured S (2,2) and de-embedded S (1,1) input reflection coefficient results are given together in Fig. 5. The input impedance measurement results of the VddPLL power supply are given in Fig. 6. The locations from which the R, L, and C values will be obtained according to these results are also indicated on the same figure.

The EMC behavior of ICs is closely linked to the presence of radiated noise in electronic systems. The noise that comes from ICs is mostly due to core activity and I/O interface switching. Models for interface stages are offered by the IBIS standard, while models for core activities are offered by the ICEM standard. These ICEM models furnish parameters necessary for simulating radiated and conducted emissions.

This method clearly defines the position and values of the uniformly radio frequency (RF) distributed current that is used to device the model, which allows us to model large complex devices too.

The value of current (complex) and the orientation angle θ (real) are designed for measurements. In this study, the Modified Genetic Algorithm is used for R, L and C values. The initial population of the Modified Genetic Algorithm (MGA) is the same as the genetic algorithm. A flowchart of how the MGA works is shown in Fig. 7.

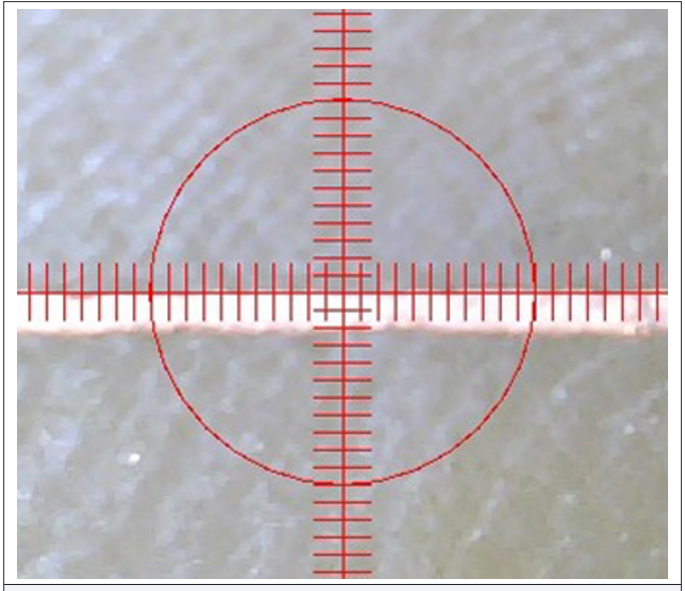

Fig. 3. The microscopic vision of the VddPLL power supply path.

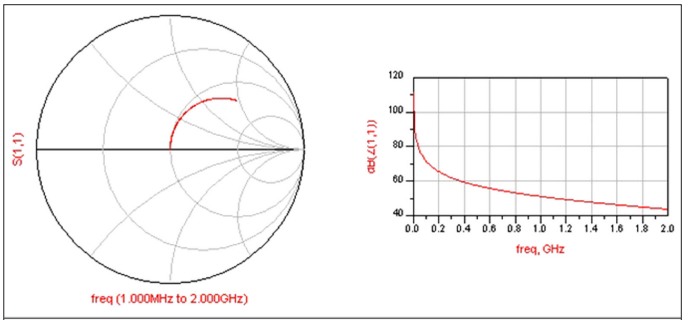

Fig. 4. Effects of the trace to the circuit.

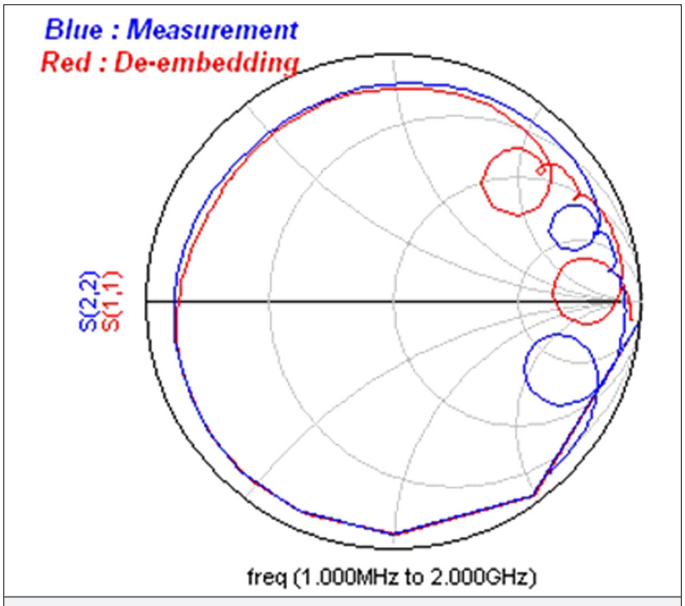

Fig. 5. Measured S (2,2) and de-embedded S (1,1) input reflection coefficient.

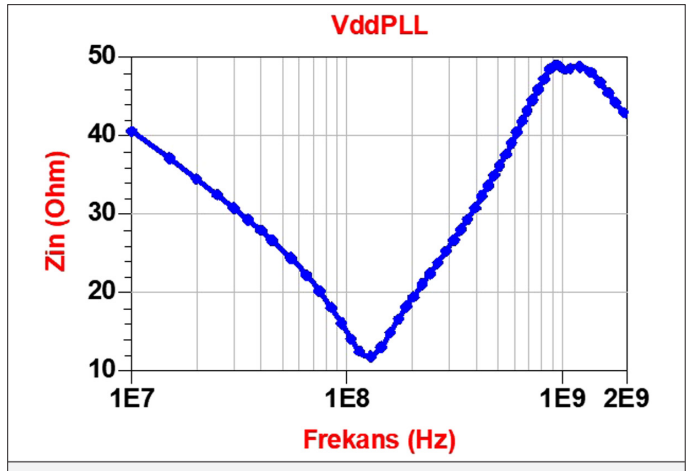

Fig. 6. Input impedance measurement results of the VddPLL power supply.

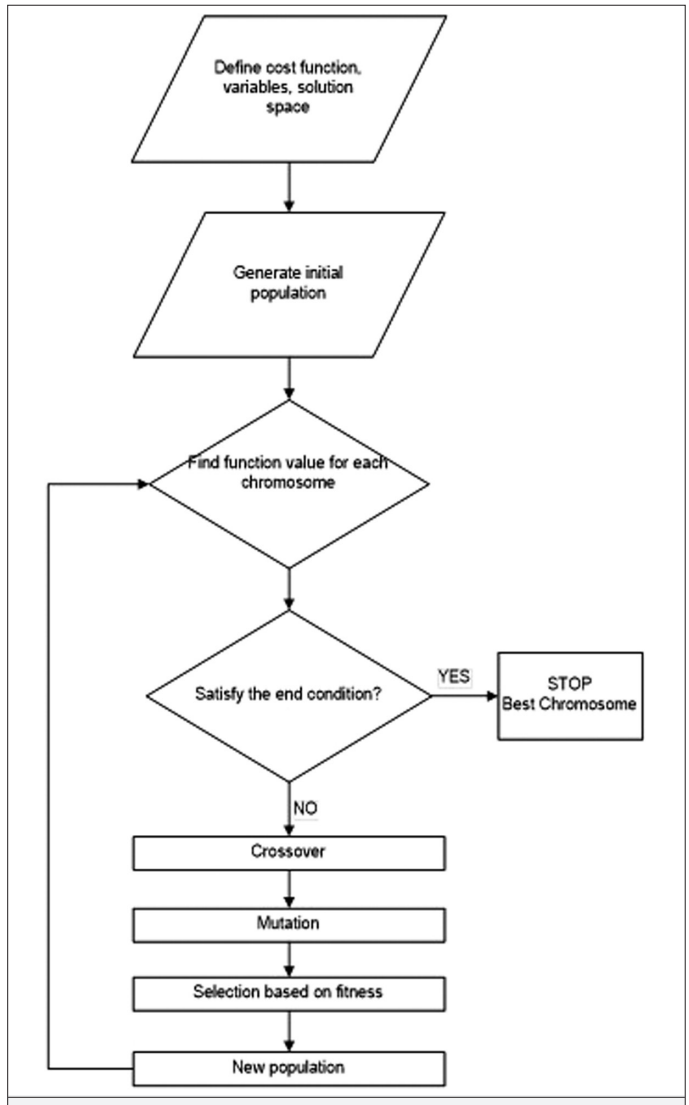

Fig. 7. Main program flowchart of modified genetic algorithm.

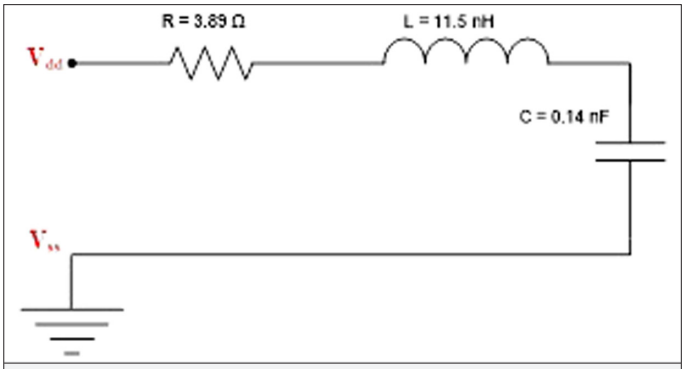

Fig. 8. The modeled passive RLC circuit.

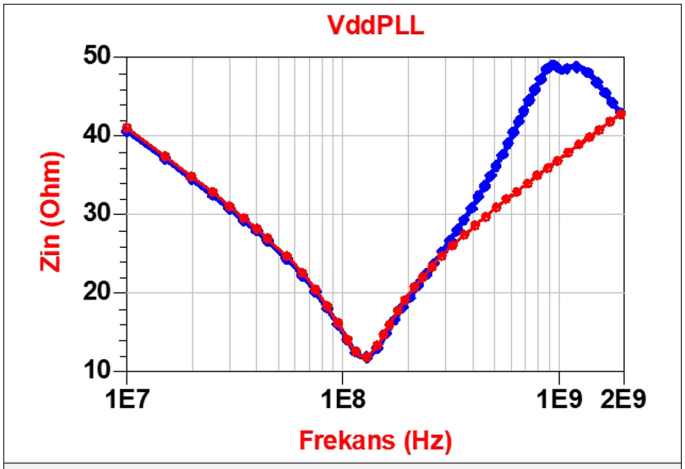

Fig. 9. Measured (blue line) and modeled by MGA impedance (red line).

$$f = \sqrt{\sum \left(\frac{Z_{\text{ölçüm}} - Z_{model}}{Z_{\text{ölçüm}}} \right)^2} \quad (1)$$

III. INTERNAL ACTIVITY MEASUREMENT

The component representing IA is defined by a parameter termed internal activity. Frequently, direct access to this parameter is not available. The transfer function of the PDN has been previously derived, and the externally flowing current, IExt, has been measured. Depending on the type of analysis required, IA can be described in either the time domain or the frequency domain.

Our measurement setup, as depicted in Fig. 10, includes a spectrum analyzer, power supply, amplifier, and S12X microcontroller. Initially, the current to be utilized in determining the external current was measured.

Port 1 is connected to the VddPLL supply pin. The current, as measured by the spectrum analyzer, has been employed to obtain the external current, as illustrated in Fig. 11.

After conducting the measurements, the results were calibrated to compensate for the amplifier's influence. The amplifier's impact was determined using a vector network analyzer, and the results, along with the degree of current amplification, are presented in Table I. By

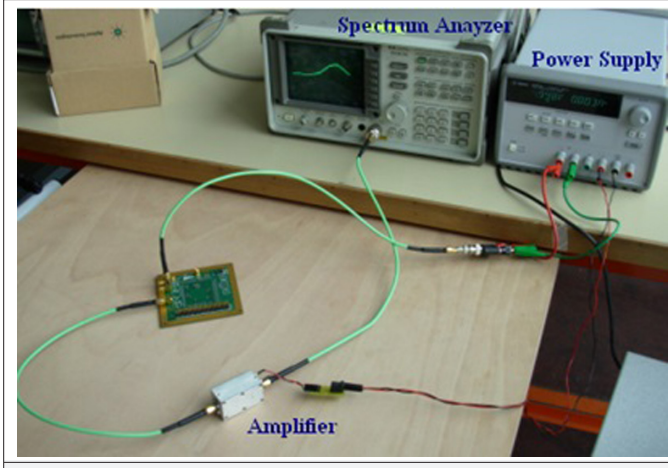

Fig. 10. Current measurement setup.

subtracting the amplified value from the measured value, the calibrated power (P_{dBm}) was obtained. To ascertain the true external current of the circuit, knowledge of the amplifier's input impedance (R_{amp}) was necessary. These input impedance values, listed in Table II, were obtained using (4) and (5). The RLC circuit modeled after MGA is shown in Fig. 8, while the curves of the circuit obtained after measurement and MGA are compared in Fig. 9.

$$P = 10^{\frac{PdBm-30}{10}} \quad (2)$$

$$V = \sqrt{2 \times P \times R} \quad (3)$$

$$I_{ext} = \frac{V}{51 + R_{amp}} + \frac{V}{50} \quad (4)$$

After determining the external current of the circuit, the internal current was derived. This involved utilizing both the PDN and the external current in the calculation process.

$$I_{\text{int}}(f) = I_{ext}(f) \times \frac{Z_{L1} + Z_{C1} + Z_{R1}}{Z_{C1}} \quad (5)$$

IV. THE PROPOSED MODEL

Designed PDN and IA components with output components of test board are shown in Fig. 12. The obtained models are added in the form of a series of RF current lines uniformly distributed along the x–y axis. For better understanding, the obtained models are placed in their state as shown in Fig. 12, to appear on an S12X circuit. The model is designed with certain parameters predetermined, including the number, length, and location of the uniformly distributed current lines. Fig. 13 provides an equivalent representation of the DUT in terms of uniform RF distributed current lines.

Using the set of equations, it becomes feasible to calculate the radiation at a specific point in space (M) by aggregating the emissions from all individual dipoles, as illustrated in Fig. 14.

It is supposed that uniformly distributed current lines are very little $(\text{I} \quad \lambda)$, very $(\text{a} \quad \lambda)$ and $(\text{I} \quad R)$; and the current on which is stable.

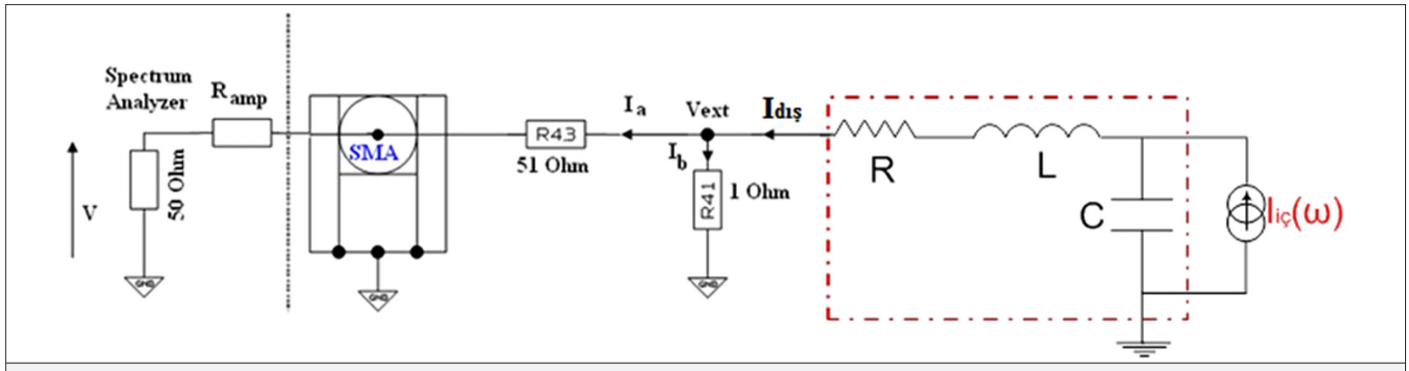

Fig. 11. The measurement configuration.

TABLE II. PASSIVE RLC CIRCUIT AND INTERNAL CURRENT VALUES FOR THE MODEL

Supply Pins	R	L	C	I_{int} 24 MHZ	I_{int} 32 MHz	I_{int} 64 MHz
V_{dd1}	1.42 Ω	106.2 nH	6.2 nF	1.7mA	2.4mA	6.8mA
V_{ddX2}	2.49 Ω	10.48 nH	0.22 nF	0.51mA	0.54mA	0.72mA
V_{ddPLL}	3.88 Ω	11.73 nH	0.14 nF	0.50mA	0.53mA	0.67mA
V_{ddR2}	1.99 Ω	10.87 pH	0.28 nF	0.51mA	0.55mA	0.77mA
V_{dd2}	1.56 Ω	8.56 nH	5.8 nF	1.6mA	2.2mA	5.7mA
V_{ddX1}	1.90 Ω	10.2 nH	0.21 nF	0.50mA	0.52mA	0.68mA
V_{ddR1}	1.51 Ω	11.58 nH	1.04 nF	0.68mA	0.81mA	1.6mA
V_{ddA}	3.74 Ω	10.49 nH	0.21 nF	0.52mA	0.56mA	0.76mA

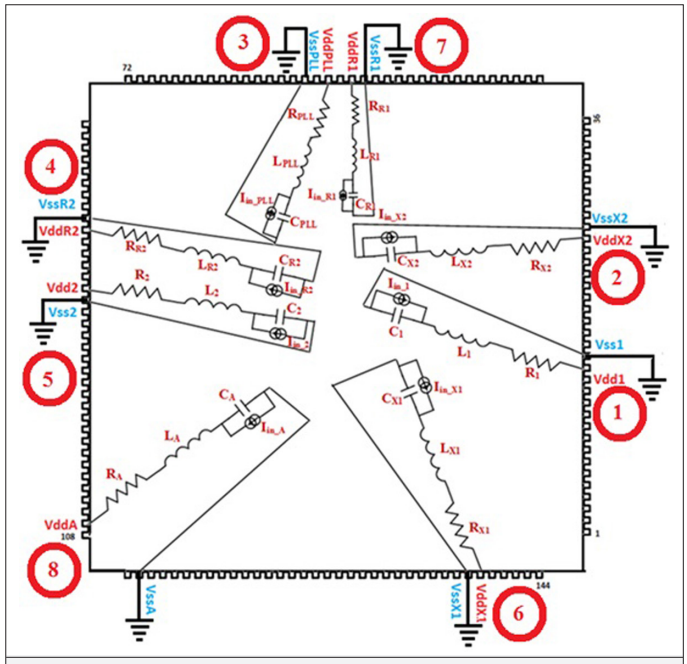

Fig. 12. The proposed model of the IC.

$$H_x = \frac{I_0}{2\pi R^2}\Delta\ell\left(\frac{z-z_0}{R}+\frac{j\omega(z-z_0)}{c}\right)\cdot sin\theta \tag{6}$$

$$H_y = \frac{-I_0}{2\pi R^2}\Delta\ell\left(\frac{z-z_0}{R}+\frac{j\omega(z-z_0)}{c}\right)\cdot cos\theta \tag{7}$$

$$H_z = \frac{I_0}{2\pi R^2}\Delta\ell\left[-\left(\frac{x-x_0}{R}+\frac{j\omega(x-x_0)}{c}\right)\cdot sin\theta+\left(\frac{y-y_0}{R}+\frac{j\omega(y-y_0)}{c}\right)\cdot cos\theta\right] \tag{8}$$

$$R = \sqrt{(x-x_0)^2+(y-y_0)^2+(z-z_0)^2} \tag{9}$$

$$H_x = \frac{I_0}{4\pi}\Delta\ell\frac{e^{-jkR}}{R^2}\left(\frac{z-z_0}{R}+\frac{j\omega(z-z_0)}{c}\right)\cdot sin\theta \tag{10}$$

$$H_y = \frac{-I_0}{4\pi}\Delta\ell\frac{e^{-jkR}}{R^2}\left(\frac{z-z_0}{R}+\frac{j\omega(z-z_0)}{c}\right)\cdot cos\theta \tag{11}$$

$$H_z = \frac{I_0}{4\pi}\Delta\ell\frac{e^{-jkR}}{R^2}\left[-\left(\frac{x-x_0}{R}+\frac{j\omega(x-x_0)}{c}\right)\cdot sin\theta+\left(\frac{y-y_0}{R}+\frac{j\omega(y-y_0)}{c}\right)\cdot cos\theta\right] \tag{12}$$

$$R = \sqrt{(x-x_0)^2+(y-y_0)^2+(z-z_0)^2} \tag{13}$$

The previously developed model clearly defines each dipole with its position, orientation, and currents. This model has been studied completely and these values that define the dipoles are computed by considering the two measurements H_x and H_y components of the magnetic field. This model is built by writing a code in MATLAB, and magnetic fields are simulated using the code.

It has been split into four major parts as listed below.

- Measurement, which deals with the measurement of the Device Under Test using the near-field test bench.
- Process of modeling.
- Simulation of the magnetic field from the model.
- Validation of the model with respect to the simulated magnetic field.

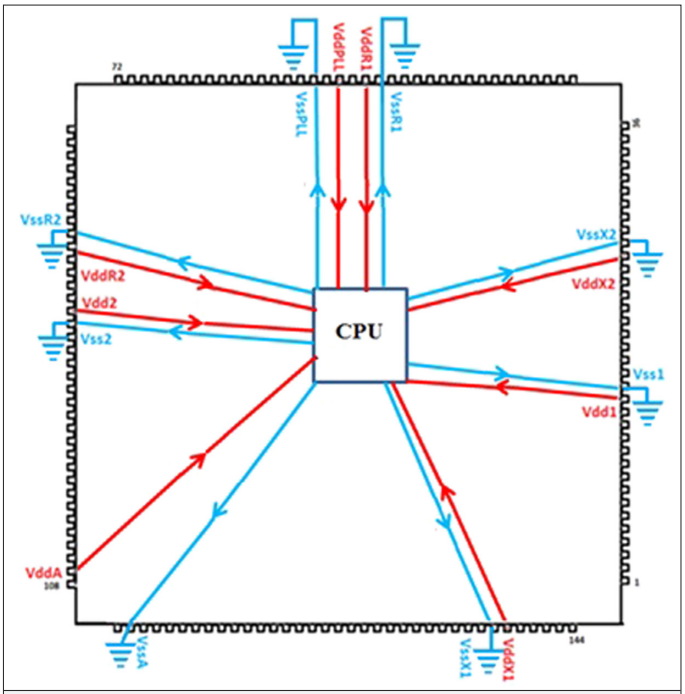

Fig. 13. The placement of the uniformly distributed current lines.

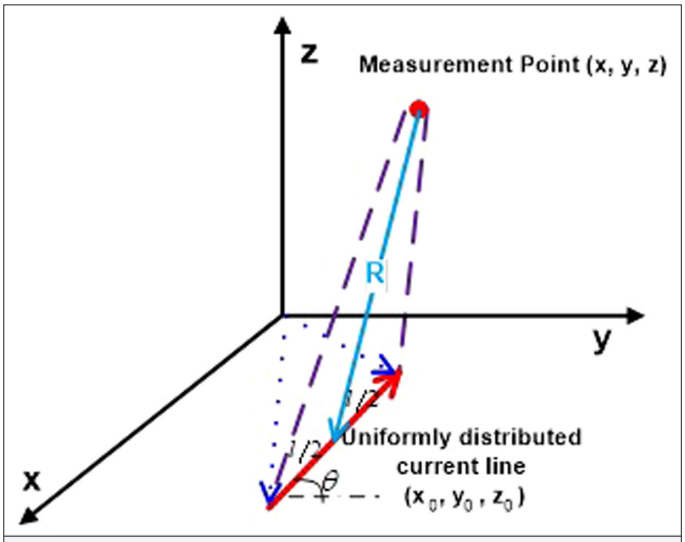

Fig. 14. Uniformly distributed current line.

The plots show us a great correlation between these three simulations, and the modeled magnetic field can be seen.

The magnetic field plots demonstrate a strong correlation between the fields emitted in all four cases, indicating that the integrated model is accurate according to our design and meets our specifications to a significant extent. However, it is not possible to achieve 100% accurate results, given the inherent differences between two distinct simulation cases. Nevertheless, the modeled domain and the domain of the integrated model are related, suggesting that the integration process is effective. A few errors do occur between simulations, but they are not significant.

In this procedure of modeling, the position and length of the uniformly distributed current lines are considered as constant, and the orientation and current for individual uniformly distributed current lines are calculated for the corresponding position and measurement point. Using the theory and equations developed in section IV, the complete model can be obtained andthe modeled magnetic fields (*x*, *y*, and *z* components) can be validated with those of the measured and/or simulated fields. Once the validation is done, the uniformly distributed currents' data (their position, orientation, and currents) are exported to a text file to integrate the model into High Frequency Simulation Software (HFSS) and validate those simulations.

Errors are minimal, and it can be concluded that the model predicts the magnetic field even though not all the sources are in the ground plane. This is a great advantage of this model because it can/could predict the magnetic field of any component.

V. MEASUREMENTS

A near-field test bench was developed to conduct real-time measurements of the device. The near-field scanner, originally adapted for ICs by K. Slattery [22], boasts a high resolution capable of mapping fields above IC packages [23]. The test bench, devised within IRSEEM to assess the electric and magnetic near fields emitted by electronic systems, is depicted in Fig. 15. The near field measurement of the S12X microcontroller has been made at different frequencies (24, 32, and 64 MHz) and different heights (h = 1 mm and h = 4 mm). The scanning surface measures 50 mm × 50 mm and is positioned at heights of 1 mm and 4 mm above the component. This surface comprises 2601 measurement points.

To achieve electromagnetic cartography, a near-field scanner and calibrated near-field probe are used. The system utilizes a direct measurement approach, where the probe is linked to a spectrum analyzer and affixed to a robotic platform. Before initiating measurements, configurations for altitude scans, scanned area, scan step, and desired frequencies are set. A computer acquires the data which is provided by the spectrum analyzer via a GPIB bus. The last step is the data storage and post-processing using data files.

These measurements have been made at three different frequencies (24 MHz, 32 MHz, and 64 MHz) and at two different heights (1 mm and 4 mm).

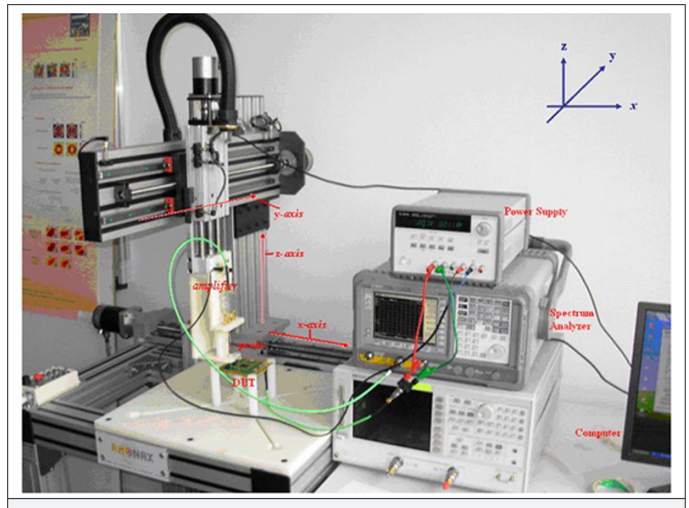

Fig. 15. Electromagnetic near-field test bench.

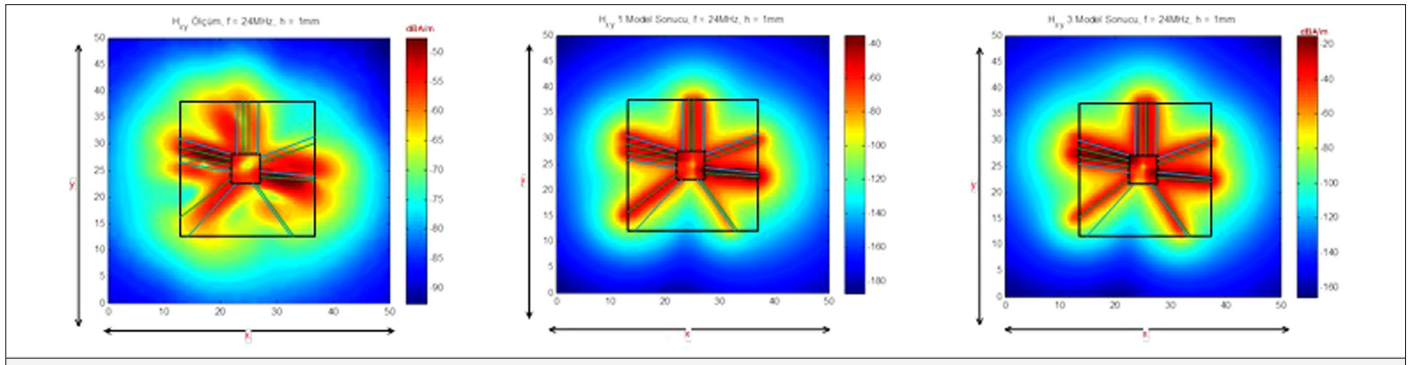

Fig. 16. 24 MHz and h = 1 mm height, magnetic field H_{xy} (dBA/m) (from left to right) measurement; 1. Model; 2. Model results.

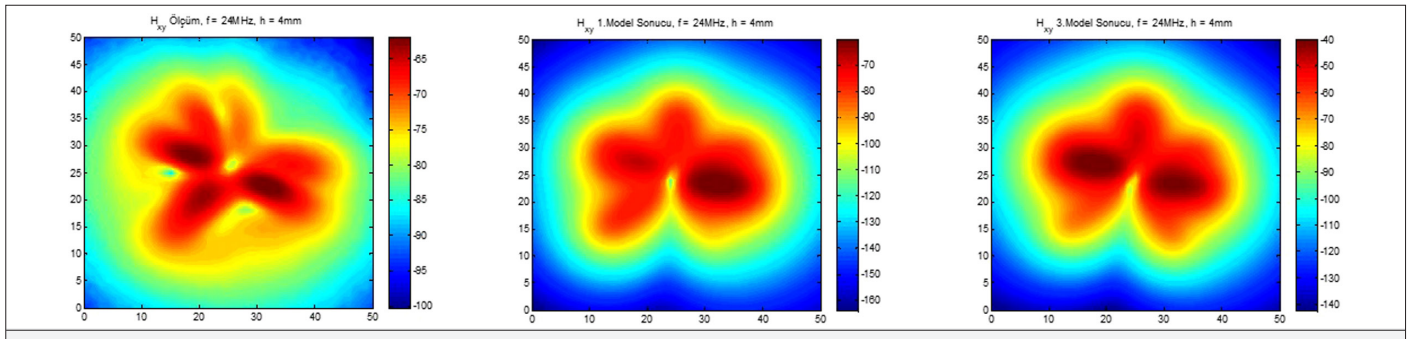

Fig. 17. 24 MHz and h = 4 mm height, magnetic field H_{xy} (dBA/m) (from left to right) measurement; 1. Model; 2. Model results.

H_{xy} component is defined in (11).

$$H_{xy} = \sqrt{H_x^2 + H_y^2} \tag{14}$$

S12X microcontroller has been used for this application. There is eight couple of power supply and ground pins on this component that is shown in Fig. 13. The measurement and two models results of the H_{xy} component are shown in Figs. 16 and 17. The findings of this study reveal significant effects of varying height and frequency values on the sensitivity of RF modules. These findings are summarized as follows:

A. Model 1

At 1 mm height and 24 MHz frequency, the error rate was measured at 0.91%.

For the same model, at 1 mm height and 32 MHz frequency, the error rate increased to 2.04%.

At 4 mm height and 64 MHz frequency, the error rate peaked at 4.69%.

B. Model 2

At 1 mm height and 32 MHz frequency, the error rate was 1.90%.

Conversely, at 4 mm height and 64 MHz frequency, the error rate dropped notably to 0.63%.

At 4 mm height and 24 MHz frequency, the error rate was measured 0.87%.

Height variation generally led to corresponding changes in error rates, with an overall trend of increasing errors with increased height. Frequency had a pronounced effect on error rates, with lower frequencies generally resulting in lower error rates, and higher frequencies yielding higher error rates.

VI. RESULTS

In this study, a new modeling method to predict the magnetic emissions of ICs has been presented. The model is based on a set of uniformly distributed current lines characterized by a value and position. It can be concluded that the model presented in this paper gives very good results and it can be used to simulate the magnetic field at any distance from the electronic component. This paper characterizes the power-distribution network using impedances. Excellent agreement was observed between the measured and simulated impedances.

The model is particularly valuable for its simplicity and swift modeling and simulation capabilities. It enables accurate simulation of the magnetic field emitted by the component under test at various distances. Operating on the principle of treating the component as a "black box," this model is versatile and applicable to both passive and active components. When modeling the emission of the IC, measurements have been taken only through power supply pins. The real-time measurement of the performance has been observed when compared with the results. The proposed model is much faster when compared with other analogies designed and error rate stands at 0.6% to 4%. Previously proposed models required longer time measurement values of two components of the magnetic fields H_x and H_y. The proposed model can obtain the magnetic fields of H_x, H_y, and H_z results at only 8 seconds. Electromagnetic emissions can be simulated at different heights above the IC. The model proposed in this study

offers fast simulation speeds and accurately captures magnetic field emissions at desired frequencies from the IC.

Peer-review: Externally peer-reviewed.

Author Contributions: Concept – M.E.B., A.K.; Design – M.E.B.; Supervision – A.K.; Resources – M.E.B.; Materials – M.E.B.; Data Collection and/or Processing – M.E.B.; Analysis and/or Interpretation – M.E.B., A.K.; Literature Search – M.E.B.; Writing – M.E.B., A.K.; Critical Review – M.E.B., A.K.

Acknowledgment: We are deeply saddened by the early loss of our esteemed doctoral advisor, Prof. Dr. Ayten Kuntman. Her guidance, wisdom, and dedication have been instrumental in shaping the careers of many scientists, including Dr. Fırat Kaçar, Dr. Aysel Ersoy Yılmaz, and Dr. Yasin Özcelep. Prof. Dr. Kuntman's profound impact on the scientific community and her unwavering support for her students will always be remembered with gratitude and admiration. We honor her memory with the deepest respect and sincerely hope that she rests in peace.

Declaration of Interests: The authors have no conflicts of interest to declare.

Funding: The authors declare that this study received no financial support.

REFERENCES

1. S. Zhao, K. Roy, and K. Cheng-Kok, "Decoupling capacitance allocation and its application to power-supply noise-aware floorplanning," *IEEE Trans. Comput. Aid. Des. Integr. Circuits Syst.*, vol. 21, no. 1, pp. 81–92, 2002. [CrossRef]
2. B. Ross, "IBIS and ICEM interaction," *Microelectron. J.*, vol. 35, no. 6, pp. 497–500, 2004. [CrossRef]
3. A. K. Varma, M. Steer, and P. D. Franzon, "Improving behavioral IO buffer modeling based on IBIS," in *IEEE Trans. Adv. Packaging*, vol. 31, no. 4, pp. 711–721, 2008. [CrossRef]
4. M. E. Başak, and A. Kuntman, "RLC circuit extraction with the differential evolution algorithm for conducted electromagnetic emission model of integrated circuits," *Turk. J. Electr. Eng. Comput. Sci.*, vol. 24, no. 1, pp. 196–205, 2016. [CrossRef]
5. Z. Zhang, and A. M. Bazzi, "A virtual impedance enhancement based transformer-less active EMI filter for conducted EMI suppression in power converters," *IEEE Trans. Power Electron.*, vol. 37, no. 10, pp. 11962–11973, 2022. [CrossRef]
6. "International Electrotechnical Commission standard IEC/TS," vol. 62404, "*Logic Digital Integrated Circuits—Specification for I/O Interface Model for Integrated Circuits (IMIC Version 1.3)*,", 2007.
7. N. Funabiki, Y. Nomura, J. Kawashima, Y. Minamisawa, and O. Wada, "A LECCS model parameter optimization algorithm for EMC designs of IC/LSI systems," in 17th International Zurich Symposium on Electromagnetic Compatibility, IEEE, vol. 2006, 2006, pp. 304–307. [CrossRef]
8. K. Ichikawa, M. Inagaki, Y. Sakurai, I. Iwase, M. Nagata, and O. Wada, *Simulation of Integrated Circuit Immunity with LECCS Model*, 2006, pp. 308–311. [CrossRef]
9. F. Lafon, O. Maurice, and F., "De-daran," *ICEM – ICIM Modeling and Exploitation for Bus Transceivers Applications*.
10. D. Capriglione, A. G. Chiariello, and A. Maffucci, *Modeling and Characterization of Parasitic Radiated Emission from a Flash Memory*, 2011, pp. 288–293.
11. C. Labussière-Dorgan *et al.*, "Modeling the electromagnetic emission of a microcontroller using a single model," *IEEE Trans. Electromagn. Compat.*, vol. 50, no. 1, pp. 22–34, Feb. 2008. [CrossRef]
12. E. Sicard, "Electromagnetic compatibility of integrated circuits," *Microelectron. J.*, vol. 35, no. 6, pp. 485–486, 2004. [CrossRef]
13. Y. Villavicencio, F. Musolino, and F. Fiori, "Electrical model of microcontrollers for the prediction of electromagnetic emissions," *IEEE Trans. Very Large Scale Integr. (VLSI) Syst.*, vol. 19, no. 7, pp. 1205–1217, 2011. [CrossRef]
14. P. Kralicek, W. John, and H. Garbe, "Modeling electromagnetic emission of integrated circuits for system analysis,", in *Proceedings -Design, Automation and Test in Europe, Date*, 2001, pp. 336–340. [CrossRef]
15. J.-R. Regue, M. Ribo, J.-M. Garrell, and A. Martin, "A genetic algorithm based method for source identification and far-field radiated emissions prediction from near-field measurements for PCB characterization," *IEEE Trans. Electromagn. Compat.*, vol. 43, no. 4, pp. 520–530, 2001. [CrossRef]
16. Y. S. Khee, and M. Z. M. Jenu, "Radiated emission of bent microstrip line using Hertzian dipole method," *IEEE Int. Symp. Electromagn. Compat.*, pp. 1–6, 2008. [CrossRef]
17. J. Ramón Pérez, and J. Basterrechea, *A Theoretical Comparison between Three Planar near to Far-Field Transformation Methods for Antenna Measurements*.
18. P. Petre, and T. K. Sarkar, "Differences between modal expansion and integral equation methods for planar near-field to far-field transformation (Summary)," *J. Electromagn. Waves Appl.*, vol. 10, no. 2, pp. 269–271, 1996. [CrossRef]
19. Y. Vives-Gilabert, C. Arcambal, A. Louis, F. de Daran, P. Eudeline, and B. Mazari, "Modeling magnetic radiations of electronic circuits using near-field scanning method," *IEEE Trans. Electromagn. Compat.*, vol. 49, no. 2, pp. 391–400, 2007. [CrossRef]
20. J.-R. Regue, M. Ribo, J. Gomila, A. Perez, and A. Martin, "Modeling of radiating equipment by distributed dipoles using metaheuristic methods," in International Symposium on Electromagnetic Compatibility, vol. 2005. EMC. IEEE Publications, 2005, pp. 596–601. [CrossRef]
21. B. Mutnury, M. Swaminathan, and J. P. Libous, "Macromodeling of nonlinear digital I/O drivers," *IEEE Trans. Adv. Packaging*, vol. 29, no. 1, pp. 102–113, 2006. [CrossRef]
22. K. P. Slattery, J. W. Neal, and W. C. W. Cui, "Near-field measurements of VLSI devices," *IEEE Trans. Electromagn. Compat.*, vol. 41, no. 4, pp. 374–384, 1999. [CrossRef]
23. A. Boyer, and S. Ben Dhia, *Electromagnetic Compatibility of Integrated Circuits*. Boston: Springer, 2006. [CrossRef]

Muhammed Emin Başak He received his BSc, MSc, and PhD degrees from Istanbul University, all in electrical and electronics engineering, in 2005, 2008, and 2014, respectively. Başak performed research from 2007 to 2008 at l'ESIGELEC, IRSEEM Institutes, Rouen, France. He is currently Associate Professor at the Faculty of Naval Architecture and Maritime at Yıldız Technical University. His general research interests include electromagnetic modeling and simulation of electronic devices and circuits.

Ayten Kuntman's academic journey at Istanbul University spans nearly three decades, commencing in 1995 as Assistant Professor and culminating in her current role as revered Professor within the Faculty of Engineering, Department of Electrical and Electronics Engineering. Throughout her tenure, Kuntman has not only excelled in teaching a diverse array of courses, including VLSI and biomedical materials but has also undertaken significant administrative responsibilities, including roles within the Institute of Graduate Studies in Sciences. Beyond her academic duties, Kuntman has left an indelible mark as a mentor, guiding numerous doctoral students and shaping the future of the field. Her scholarly achievements are matched only by her warmth and approachability, ensuring that she is fondly remembered by colleagues and students alike. Ayten Kuntman's legacy extends far beyond her research, embodying the ideals of excellence and kindness that continue to inspire generations of scholars within the academic community.